COMPUTED TRANSIENT SUPERCAVITATING FLOW OVER A PROJECTILE

Nabil H. Mostafa

Mechanical Power Department, College of Engineering
Zagazig University, Zagazig, 44519, Egypt
E-mail: nmostafa@vt.edu

ABSTRACT

Supercavitation has a great effect on the design of high-speed underwater vehicles. The transit flow around either partially cavitating or supercavitating body affects the trajectory of high-speed underwater vehicles.

To improve the understanding of the unsteady behavior of supercavitating flows, the author used a three-dimensional Navier-Stokes code (CFDRC, 2000) to model the two-phase flow field around a hemisphere cylinder. The governing equations are discretized on a structured grid using an upwind difference scheme. For different body shapes and cavitation numbers, the cavity shape was determined over the body and around the wake. Also, the two-dimensional flowfield around the cavitating body was determined. This hemisphere cylinder body has a diameter about 0.2 times its length (0.2L) for the case of the hemisphere from both sides and 0.4L for the case of hemisphere from one side; so, it has a strong wake effect. The macroscopic behavior of the formation and transport of vapor bubbles are discussed with the effect of the pressure, velocities and turbulent distribution. The results show that there are five stages for the cavities formation. First, a cavity starts to grow at the wake of the body only due its low pressure. At the second stage, another cavity grows beside the nose while growing the cavity at the body wake. The cavity beside the nose grows enough to affect the pressure at the body wake, so, the cavity at the body wake starts to collapse at the third stage. In the fourth stage, the cavity beside the nose grows enough to merge with the cavity at the body wake forming a large one. Finally, that cavity starts to have a fluctuation around the final shape. The results were compared with the experimental results obtained with Particle Image Velocimetry (PIV) by the author (2001). The results show great detailed views and analysis of different fields of transit cavitating flow. It illustrates clearly the mechanism of stabilization of the cavitation behaviour provided by high-speed underwater vehicles.

Key Words: Supercavitation, Hydrofoils, CFD and Two-Phase Flows.

INTRODUCTION

Many studies of cavitation were carried out during the last three decades, (Knapp,

1970, Hammitt, 1980, and Mostafa et al. 1990). A theoretical and numerical model was developed to describe the unsteady behavior of cavitation, including vapor cloud shedding around 2D- hydrofoils by Redoud et al. (1999). They analyzed the transient pressure and velocity fields. A numerical model, previously developed at LEGI to describe the unsteady behavior of cavitation was applied to the 2D- hydrofoils geometry. Fine and Kinnas (1993) determined the cavity extent and shape for a given cavitation number by satisfying the three-dimensional kinematic and dynamic boundary conditions on the hydrofoil surface underneath the cavity and on the portion of the wake sheet that overlaps with the cavity. The flow around either partially cavitating or supercavitating hydrofoils are treated by Kinnas et al. (1994) with a viscous/inviscid interactive method. The effect of Reynolds number on the predicted cavity extent and volume for a given cavitation number were correlated with either the angle of attack or the lift coefficient. Kunz et al. (1999) presented an implicit algorithm for the computation of two-phase viscous flows. The baseline differential equation system is the multi-phase Navier-Stokes equations, comprised of the mixture volume, the mixture momentum, and the constituent volume fraction equations, but this system does not include the effect of the body wake.
The velocity field around a high-speed supercavitating body has been successfully measured using the Digital Particle Image Velocimetry (DPIV) by Mostafa et al. (2001). High-speed supercavitation has been realized in a shooting arrangement, which overcomes drawbacks of the cavitation tunnel. The bubble shape is determined by analyzing the intensity of the laser sheet.

The object of this work is to study the transit flow around either partially cavitating or supercavitating body affect the trajectory of high-speed underwater vehicles, which have strong wake effect. To improve the understanding of the unsteady behavior of supercavitating flows, the author used a three-dimensional Navier-Stokes code (CFDRC, 2001) to model the two phase flow field around a hemisphere cylinder. This body has a diameter about 0.2L to 0.4L. The governing equations are discretized on a structured grid using an upwind difference scheme. For different body shapes and cavitation numbers, the cavity shape over the body and around the wake and the two-dimensional flowfield around the cavitating body are determined.

THEORY BACKGROUND

The basic approach is to use standard viscous flow (Navier-Stokes) equations with provisions for variable density and a conventional turbulence model, such as K-ε model. A numerical model previously developed by CFDRC to solve Navier-Stokes equations (Sighal, 1999).

The mixture density (ρ) is a function of vapor mass fraction (f), which is computed by solving a transport equation simultaneously with the mass and momentum conservation equations. The ρ -f relationship is:

$$\frac{1}{\rho} \equiv \frac{f}{\rho_v} + \frac{1-f}{\rho_1} \tag{1}$$

In two-phase flows, the use of vapor volume fraction (α) is also quite common. Therefore, it is deduced from f as follows:

$$\alpha = f\frac{\rho}{\rho_v} \tag{2}$$

The transport equation for vapor is written as follows:

$$\frac{\partial}{\partial t}(\rho f) + V \bullet (\rho \vec{V} f) = V \bullet (\Gamma \nabla f) + R_e - R_c \tag{3}$$

The expressions of R_e and R_c have been derived from the reduced form of the Rayleigh-Plesset equation (Hammitt, 1980), which describes the dynamics of single bubble in an infinite liquid domain. The expressions for R_e and R_c are:

$$R_e = C_e \frac{V_{ch}}{\sigma} \rho_l \rho_v \sqrt{\frac{2}{3}\frac{p_{sat} - p}{\rho_l}(1-f)} \tag{4}$$

$$R_c = C_c \frac{V_{ch}}{\sigma} \rho_l \rho_v \sqrt{\frac{2}{3}\frac{p - p_{sat}}{\rho_l}} f \tag{5}$$

Cavitation normally takes place in the vicinity of low pressure (or locally high velocity) regions, where turbulence effects are quite significant. In particular, turbulent pressure fluctuations have significant effect on cavitating flows. The magnitude of pressure fluctuations is estimated by using the following empirical correlation (Hinze, 1975):

$$P'_{turb} = 0.39\, \rho\, k \tag{6}$$

The phase-change threshold pressure value is as:

$$p_v = p_{sat} + 0.5 p'_{turb} \tag{7}$$

It is well known that cavitating flows are sensitive to the presence of non-condensable gases. In most liquids, there is a small amount of non-condensable gases present in dissolved and/or mixed state. For example, laboratory water generally has 15 ppm air dissolved in it. In other applications, e.g., marine propellers, etc., this amount may be considerably larger. In this model, the non-condensable gas is included by prescribing an estimated mass fraction at inlet. This value is held constant throughout the calculation domain. However, the corresponding density (and hence volume fraction) varies significantly with local pressure. The perfect gas law is used to account for the expansion (or compressibility) of gas; i.e.

$$\rho_{gas}=\frac{WP}{RT} \tag{8}$$

The calculation of mixture density (Equation 1) is modified as:

$$\frac{1}{\rho}=\frac{f_v}{\rho_v}+\frac{f_g}{\rho_g}+\frac{1-f_v-f_g}{\rho_l} \tag{9}$$

We have the following expression for the volume fractions of vapor (α_v) and gas (α_g):

$$\alpha_v=f_v\frac{\rho}{\rho_v} \tag{10}$$

$$\alpha_g=f_g\frac{\rho}{\rho_g} \tag{11}$$

and,

$$\alpha_l=1-\alpha_v-\alpha_g \tag{12}$$

The combined volume fraction of vapor and gas (i.e., $\alpha_v + \alpha_g$) is referred to as the Void Fraction (α). In practical applications, for qualitative assessment of the extent and location of cavitation, contour maps of void fraction (α) are important.

RESULTS AND DISCUSSION

The transient cavitation flow analysis is computed for different cavitation numbers. There are two sets of results that are computed for two hemispherical cylinders. The first hemispherical cylinder has half sphere from one side and the other has half sphere from both sides. Two different structured grids are used as shown in Figure 1. In the case of hemispherical cylinder from two sides, a one 2D block is used as shown in Figure 1a. The structure grids are divided into three faces, arch of 50 x 45 grid points, rectangular of 100 x 45 grid points and arch of 50 x 45 grid points. In the case of hemispherical cylinder (one side), two 2D blocks is used as shown in Figure 1b, so, this uses the multiblock system. The structure grids are divided into four faces arch of 60 x 40 grid points, and rectangulars of 50 x 40, 40 x 40 and 10 x 40 grid points. The grids are clustered near the body to solve the boundary layer. The length of the grid in physical domain is about three times the body length. The physical time step is taken to be $1x10^{-4}$ or $1x10^{-5}$ second for the unsteady flow computations in order to resolve accurately the transients of the supercavitating flow.

Figure 2 displays the iso-density contours for cavitating flow over the hemispherical body in a time sequence of the bubble shape. This hemisphere cylinder has half spheres from both sides with diameter 0.2 L. The cavitation number is σ = 0.0555 at

speed of u = 60 m/s. It is demonstrated that the cavity formation has five stages. First, a cavity starts to grow at the wake of the body only due to its low pressure as shown in Figures 2a and b. At the second stage, another cavity grows beside the nose while the cavity at the body wake continues to grow as shown in Figures 2b and c. The cavity beside the nose grows enough to affect the pressure at the body wake, so, the cavity at the body wake starts to collapse at the third stage as shown in Figures 2c and d. In the fourth stage, the cavity beside the nose grows enough to merge with the cavity at the body wake forming a large one as shown in Figures 2e, f and g. Finally, that cavity starts to have a fluctuation around the final shape as shown in Figure 2h.

Figure 3 represents the void fraction, turbulence kinetic energy, total pressure, pressure and velocities (u and v) in the last condition in Figure 2. The void fraction contour is approximately similar to the iso-density contours as well as the iso-total pressure contours. There is a reverse flow in the horizontal velocity component at the cavities region near to the body and in the body wake. The maximum vertical velocity component is concentrated around the front nose. In this case, the maximum turbulence kinetic energy is around the front nose similar to the iso-pressure contour.
Figure 4 demonstrates the cavities formation at a speed of 30 m/s and $\sigma = 0.22$ on the same previous body and grids. This figure demonstrates the first three stages of cavity formation. The cavity is generated and growth in the body wake only in the first stage as shown in Figures 4a and b. In the second stage, the bubble starts to be generated beside the front nose in the same time like the bubble in the body wake as shown in Figures 4b, c and d. In the third stage, the cavity beside the nose grows enough to affect the pressure at the body wake, so, the cavity at the body wake starts to collapse at the third stage as shown in Figures 4d, e and f. In this case, the merging between the two cavities does not be reached, but the shape oscillation in the final shape occurs as shown in Figure 4 f and g.

Figure 5 presents the void fraction, turbulence kinetic energy, total pressure, pressure and velocities (u and v) in the last condition in Figure 4. The void fraction contours are approximately similar to the iso-density contours as well as the iso-total pressure contours. There is a reverse flow in the horizontal velocity component at the cavities region near the body and in the body wake. The maximum vertical velocity component is concentrated around the front nose. In this condition, the maximum turbulence kinetic energy is around the front nose and at the end of the front cavity in the middle of the body.

Figure 6 demonstrates the cavities formation on hemispherical cylinder at a speed of 30 m/s and $\sigma = 0.22$. This hemisphere cylinder has half sphere at front side only with diameter 0.4 L. This figure demonstrates the five stages of cavity formation. First, a cavity starts to grow at the wake of the body only due to its low pressure as shown in Figures 6a and b. At the second stage, another cavity grows beside the nose while the cavity at the body wake continues to grow as shown in Figures 6b and c. The cavity beside the nose grows enough to affect the pressure at the body wake, so, the cavity at the body wake starts to collapse at the third stage as shown in Figures 6c and d, but not to the limit happened in the hemispherical cylinder at both sides. In the fourth stage,

the cavity beside the nose grows enough to merge with the cavity at the body wake forming a large one as shown in Figures 6d, e and f. Finally, that cavity starts to fluctuate around the final shape as shown in Figure 6g and h.

Figure 7 demonstrates the comparison between experimental and computational cavity forming on hemisphere cylinder at a speed of 30 m/s and $\sigma = 0.22$. This hemisphere cylinder has half sphere from front side only at diameter 0.4L. Figure 7b shows a frame of a supercavitating hemisphere cylinder obtained with a shutter time 1/1000 sec. The extension of the bubble in the back is due to the limited speed of the shutter time. The bubble view and cavity shape show good agreement between both of them.

SUMMARY AND CONCLUSIONS

The transit flow around either partially cavitating or supercavitating high-speed underwater vehicles is affected by its wake. This hemisphere cylinder body has a diameter about 0.2 times its length (0.2L) for the case of the hemisphere from both sides and 0.4L for the case of hemisphere from one side; so, it has a strong wake effect.

There are five stages for the cavities formation. First, a cavity starts to grow at the wake of the body only due its low pressure. At the second stage, another cavity grows beside the nose while the cavity at the body wake continues to grow. The cavity beside the nose grows enough to affect the pressure at the body wake, so, the cavity at the body wake starts to collapse at the third stage. In the fourth stage, the cavity beside the nose grows enough to merge with the cavity at the body wake forming a large one. Finally, that cavity starts to fluctuate around the final shape. There is a reverse flow in the horizontal velocity component at the cavities region near to the body and in the body wake. The maximum vertical velocity component is concentrated around the front nose. In case if the front cavity does not merge with the body wake cavity the maximum turbulence kinetic energy will be around the front nose and at the end of the front cavity in the middle of the body. The cavitation model is in a very good agreement with the experimental data.

NOMENCLATURE

C_e, C_c	phase change rate coefficients	
D	projectile diameter	m
f	vapor mass fraction	
L	projectile length	m
κ	turbulence kinetic energy	m^2/s^2
P	fluid static pressure	N/m^2
p_{sat}	saturation pressure	N/m^2
P'_{turb}	magnitude of pressure fluctuations	N/m^2
P_t	total pressure	N/m^2
R	universal gas constant	Nm/kg.K

R	rate of phase change	
R_{en}	Reynolds number	
T	fluid temperature	K
Δt	physical time step	second
u,v,w	velocity in x, y, and w directions respectively	m/s
$\vec{V}$	velocity vector	
V_{ch}	characteristic velocity $V_{ch} = \sqrt{\kappa}$	
W	molecular weight	kg/kg-mol

GREEK LETTERS

α	vapor volume fraction	
Γ	effective exchange coefficient	
ρ	mixture density	kg/m^3
σ	cavitation number $((p_\infty - p_v)/(1/2\rho_l u^2))$	N/m

SUFFIXES

c	bubble reduction and collapse
e	bubble generation and expansion
gas, G	gas phases
l	liquid phases
v	vapor phases

REFERENCES

CFDRC "CFD-ACE+ Theory and Users' Manuals, Ver. 6.4", January, 2000.

Fine, N. and Kinnas, S. A., 1993, "A Boundary Element Method for the Analysis of the Flow around 3-D Cavitating Hydrofoils," *Journal of Ship Research*, Vol. 37, No. 3, pp. 213-224.

Hammitt, F. G., 1980, *Cavitation and Multiphase Flow Phenomena*, McGraw-Hill International Book Co., New York.

Hinze, J. O., 1975, *Turbulence*, McGraw-Hill Book Co., Second Edition.

Knapp, R. T., James, D. W. and Hammitt, F. G., 1970, *Cavitation*, McGraw-Hill, New York.

Kinnas, S. A. and Fine, N. E., 1993, "A Numerical Nonlinear Analysis of the Flow around Two- and Three-Dimensional Partially Cavitating Hydrofoils," *J. Fluid Mech.,* Vol. 254, pp. 151-181. Cambridge University Press.

Kinnas, S.A., Mishima, S., Brewer, W.H., 1994, "Non-Linear Analysis of Viscous Flow around Cavitating Hydrofoils," *Twentieth Symposium on Naval Hydrodynamics,* University of California, Santa Barbara, CA.

Kunz, R. F., Boger D. A., Stinebring, D. R., Chyczewski, T. S., and Gibeling H. J., 1999, "A preconditioned Navier-Stokes Method for Two-Phase Flows with Application to Cavitation Prediction," *AIAA-99-3329,* pp. 676-688.

Mostafa, N. H., Rayan, M. A., and Mahgob, M. M., 1990, "Energetic Model for Cavitation Erosion Prediction in Centrifugal Pump Impeller," *Proceeding of ASME/CSME Cavitation and Multiphase Flow Forum,* Toronto, Canada, pp. 133-138.

Mostafa, N. H., Nayfeh, A., Vlachos, P., and Telionis, D., 2001, "Cavitating Flow over a Projectile," *39th AIAA Aerospace Science Meeting and Exhibit, 2001-1041*, Reno, Nevada,

USA.

Reboud, J., Fortes-Patella, R., Hofmann, M., and Lohrberg, H., 1999, "Numerical and Experimental Investigations on the Self-Oscillating behavior of Cloud Cavitation" "Part 2: Dynamic Pressure," *Proceeding of the 3rd ASME/JSME Joint Fluid Engineering Conference*, San Francisco, California, FEDSM99-6755.

Sighal, A. K., 1998, "Key Elements of Verification and Validation of CFD Software," AIAA98-2639, *29th AIAA, Fluid Dynamic Conference*, Allbuqurqe, NM, June 15-18, 1998.

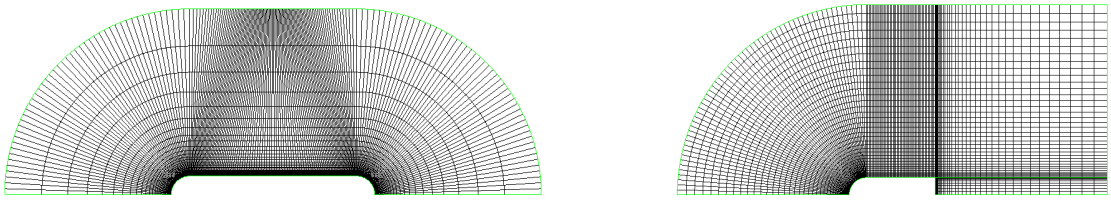

a) Hemispherical cylinder from both sides **b) Hemispherical cylinder from single side**

Fig. (1) The structured grids over a hemispherical cylinder

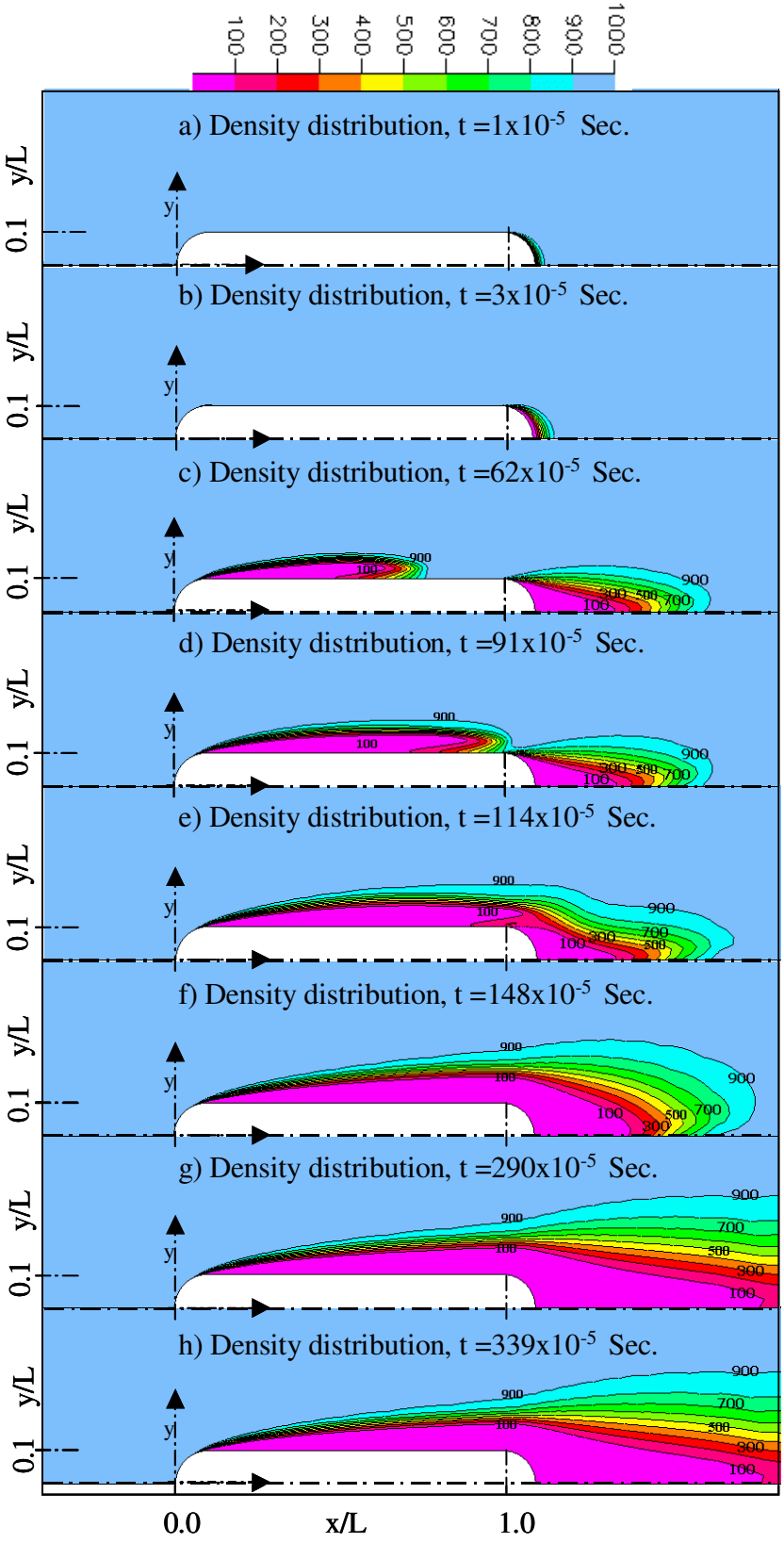

Fig. (2) supercavitating cavities formation upon hemisphere cylinder from both sides at D/L=0.2, σ =0.0555, u= 60 m/s, R_{en}=306 x10^6 and time step Δt = 10^{-5} sec.

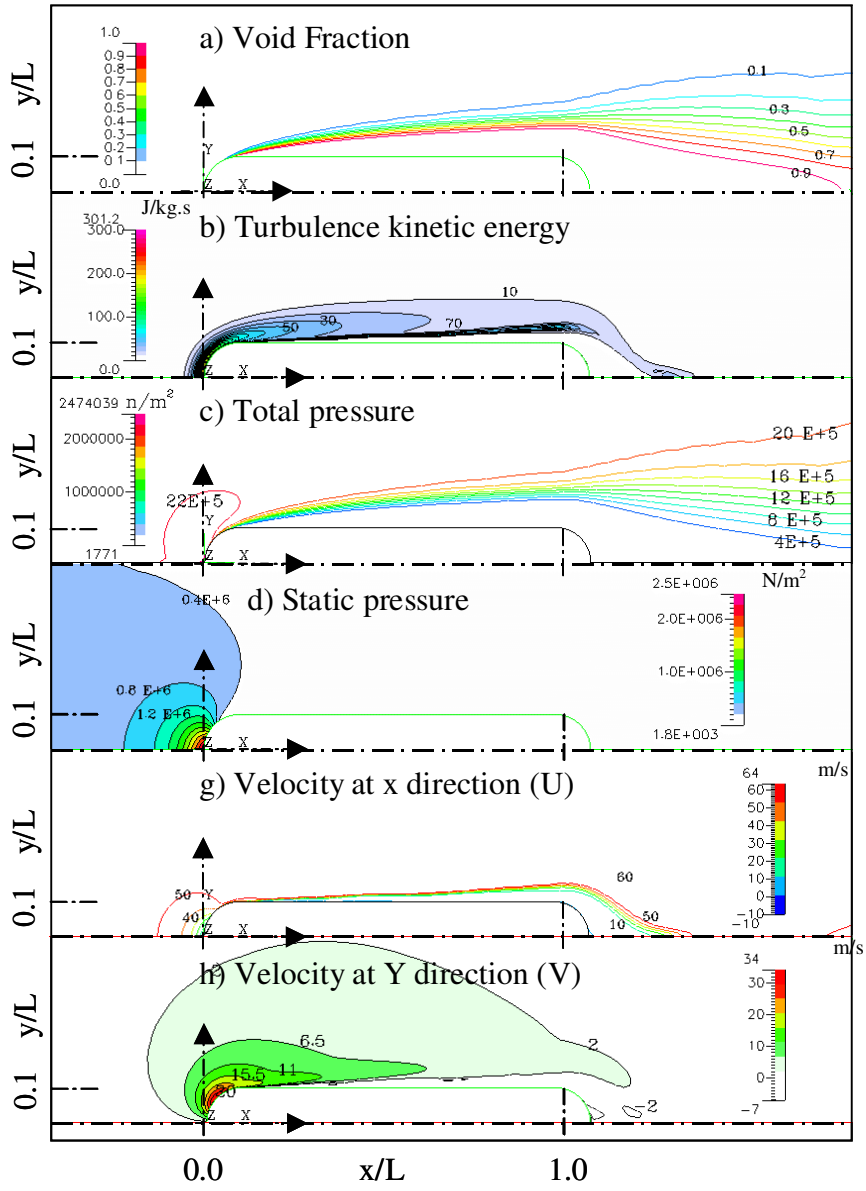

Fig. (3) Flow condition around hemisphere cylinder from both sides at supercavitating condition, D/L = 0.2, σ = 0.0555, u = 60 m/s, R_{en} = 306 x10^6, and t = 0.0034 sec.

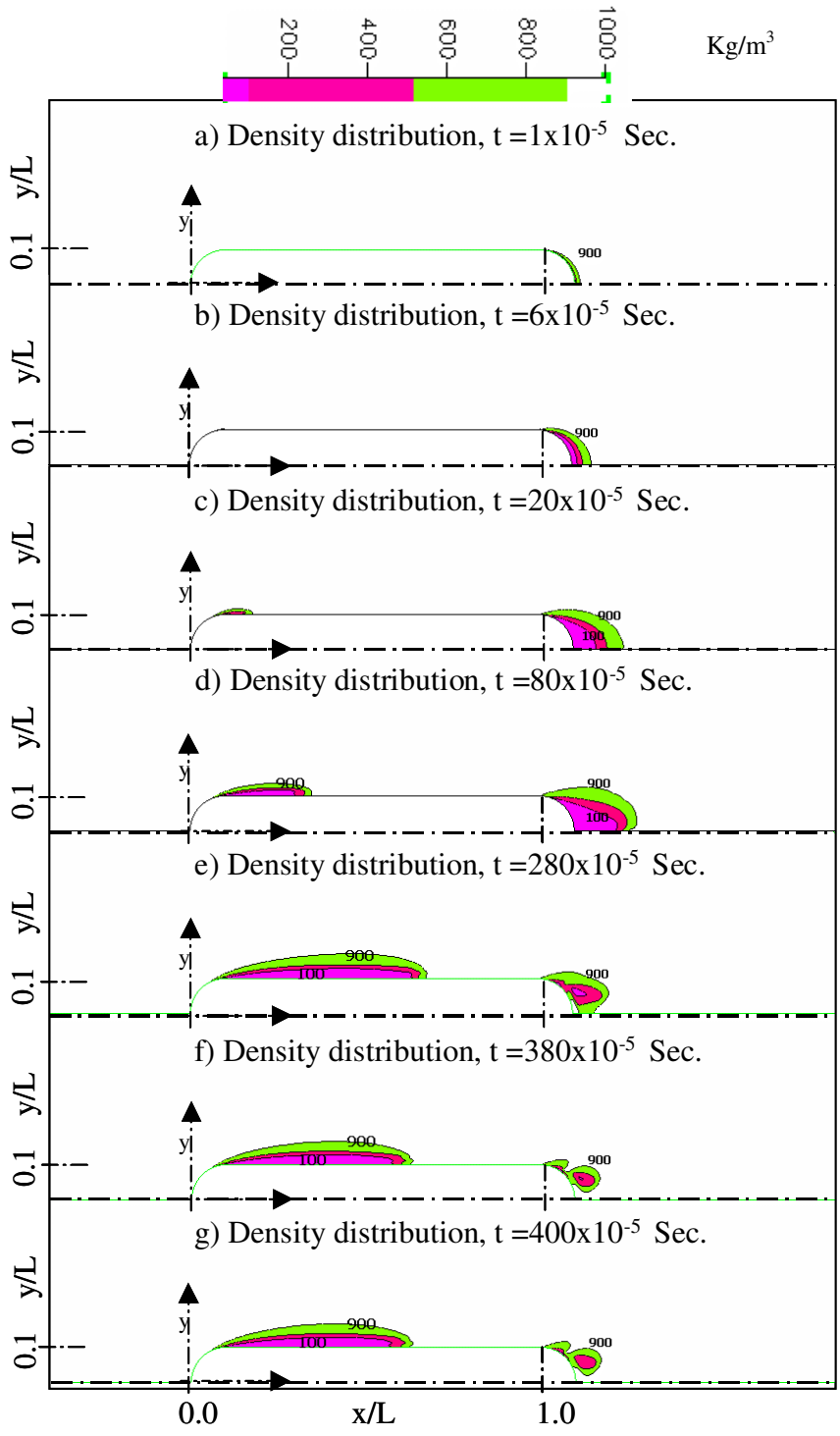

Fig. (4) Supercavitating formation upon hemisphere cylinder from both sides at D/L = 0.2, σ = 0.22, u = 30 m/s, R_{en} = 153 x 10^6 and time step Δt = 10^{-5} sec.

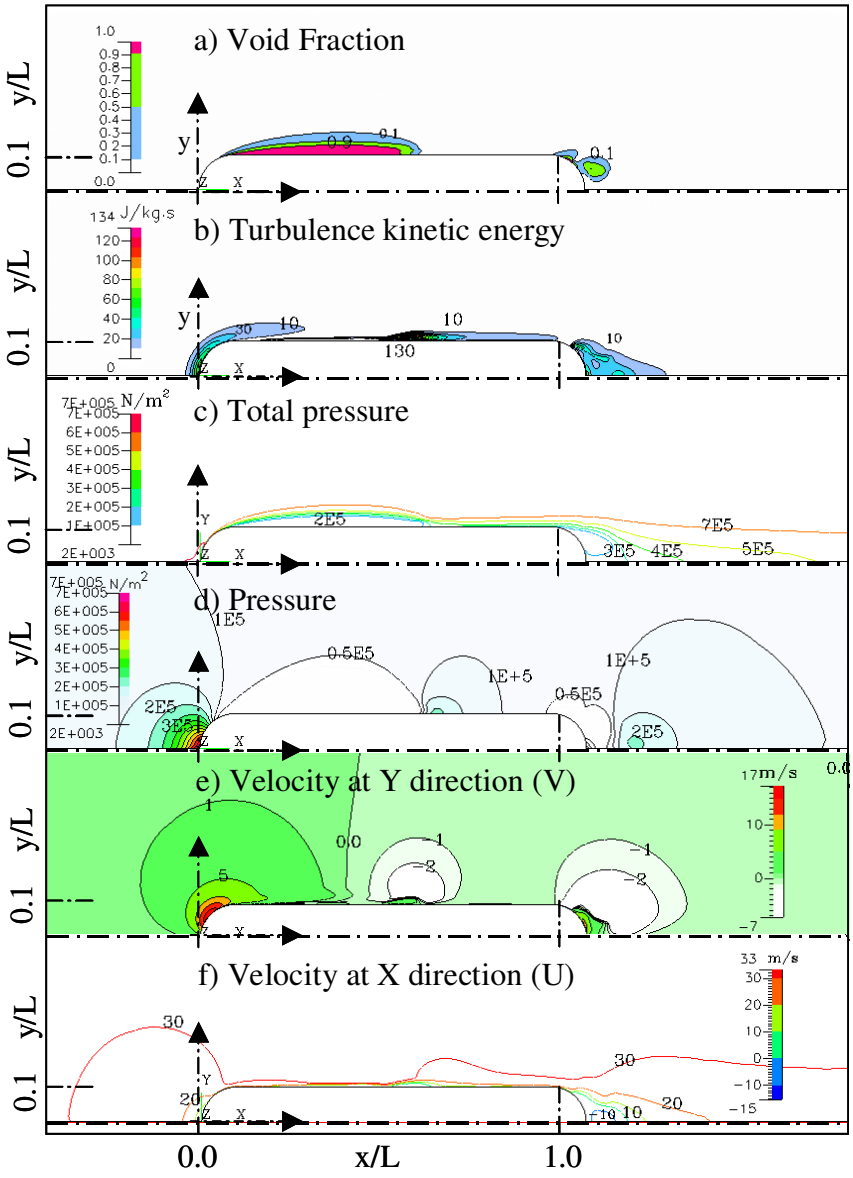

Fig. (5) Flow condition around hemisphere cylinder from both sides at supercavitating condition, D/L = 0.2, σ = 0.22, u = 30 m/s, R_{en} = 153 x 10^6, and t = 0.0038 sec.

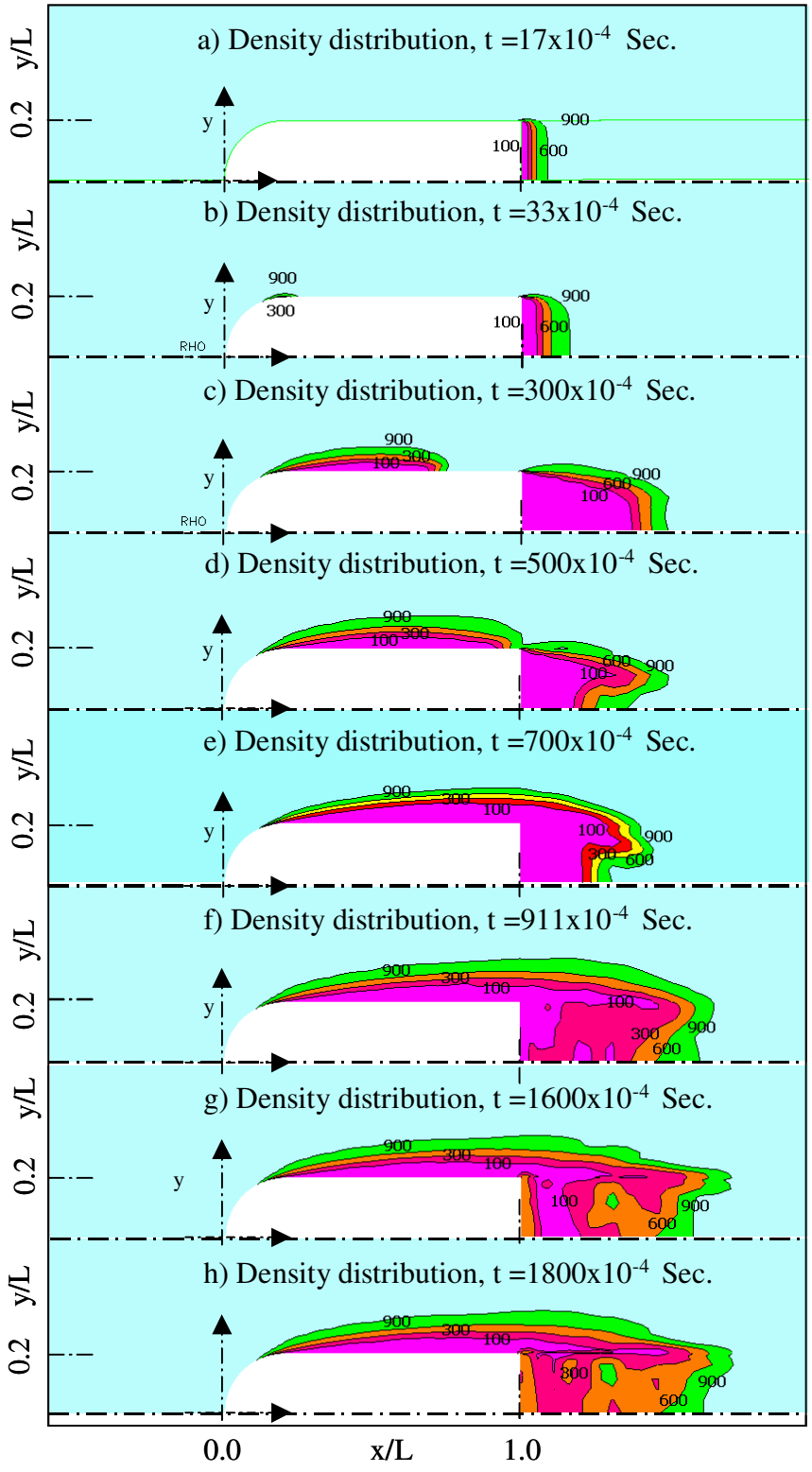

Fig. (6) Supercavitating formation upon hemisphere cylinder from one side at D/L = 0.4, σ = 0.22, u = 30 m/s, and R_{en} = 153 x 10^6.

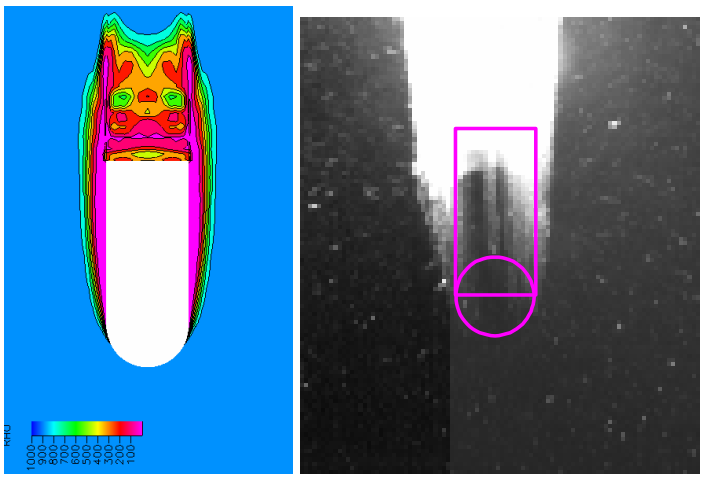

a) Computational cavity **b) Experimental cavity, Mostafa et al. (2001)**

Fig. 7. Comparison between experimental and computational cavities forming onto hemisphere cylinder body at a speed of 30 m/s and cavitation number, σ = 0.22.